



All adjacent seas of the Pacific Ocean are grouped along its west coast. Some of them (such as the Arafura and East China Seas) are large shelf seas, others (e.g. the Solomon Sea) deep basins. In contrast to the situation in the Indian and Atlantic Oceans, adjacent seas of the Pacific Ocean exert little influence on the hydrology of the main ocean basins. The Australasian Mediterranean Sea, the only mediterranean sea of the Pacific Ocean, is a major region of water mass formation and an important element in the mass and heat budgets of the world ocean; but its influence on Pacific hydrology is of only minor importance, too, far less than its effect on the hydrology of the Indian Ocean.

Before considering the Pacific topography in detail it is worth looking at the world ocean as a whole. Figure 8.1 shows that a system of inter-oceanic ridges, the result of tectonic movement in the earth's crust, structures the world ocean into a series of deep basins. The major feature of this system is a continuous mountain chain that stretches from the Arctic Mediterranean Sea through the Atlantic and Indian Oceans into the Pacific Ocean and ends in the peninsula of Baja California. Numerous fracture zones cut deep into the slopes of this chain. To map them all in reliable detail will require an enormous amount of ship time and remains a task of the future. In the large-scale maps of this book the details cannot be shown anyway, but they are important where they connect deep basins which would otherwise be isolated. To give an idea of the real topography, Figure 8.2 gives an example of such a fracture zone from the Atlantic Ocean, on the original scale of the GEBCO charts. It is obvious that the world ocean has not been surveyed to that amount of detail and many passages for the flow of bottom water are not accurately known.

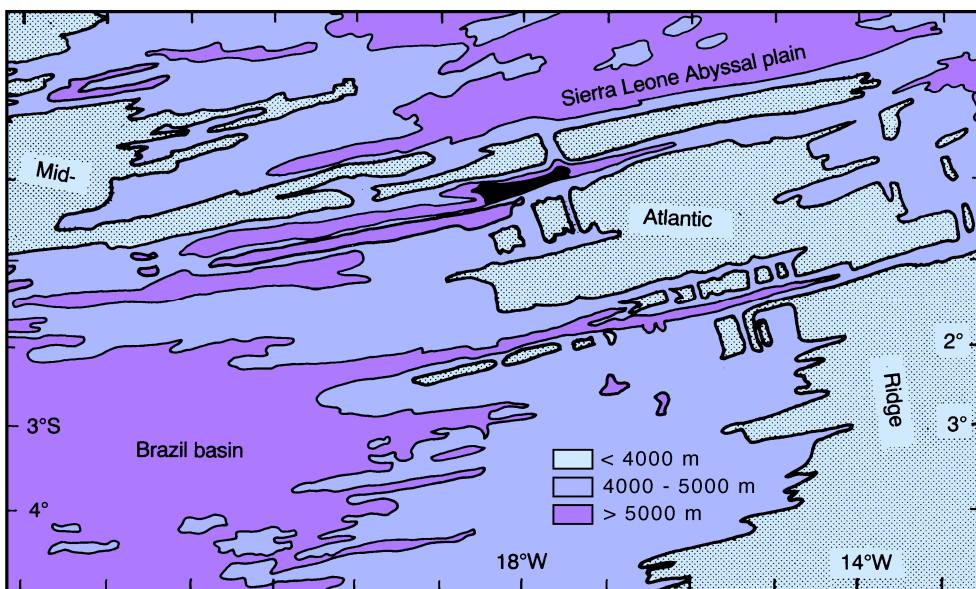


Fig. 8.2. An example of fracture zones in the inter-oceanic ridge system. the Mid-Atlantic Ridge at the equator. The ridge stretches from northwest to southeast as a series of depths <4000 m. It is cut by the Romanche Fracture Zone at the equator (identifiable by the Romanche Deep with depths >6000 m, shown in black) and the Chain Fracture Zone at 2° - 3°S. Two other fracture zones can be seen north of the equator. The figure is a simplified reproduction of part of a GEBCO chart, on the same scale.



is subdivided more by convention than topography into the *Northeast Pacific*, *Northwest Pacific*, *Central Pacific*, and *Southwest Pacific Basins* (Figure 8.3). Further west, New Zealand and the Melanesian islands provide a natural boundary for two adjacent seas of the Pacific Ocean, the Tasman and Coral Seas, while in the north the *West* and *East Mariana Ridges* and the *Sitito-Iozima Ridge* offer a natural subdivision.

Communication between the Southern Ocean and the Pacific basins is much more restricted by the topography than in the other oceans. Flow of water from the Australian-Antarctic into the Southwest Pacific Basin and the Tasman Sea is blocked below the 3500 m level. Flow from the Amundsen Abyssal Plain into the Southwest Pacific Basin is possible to somewhat greater depth but not below 4000 m. The *Peru* and *Chile Basins* are closed to the north and west at the 3500 m level but connected with the *Mornington Abyssal Plain* and with each other at slightly greater depth, probably somewhere around 3600 - 3800 m.

A unique feature of the Pacific Ocean is its large number of seamounts, particularly in the Northwest and Central Pacific Basins. Seamounts are found in all oceans, but the volcanism of the northwestern Pacific Ocean produces them in such numbers that in some regions they cover a fair percentage of the ocean floor (Figure 8.4). This may have an impact on the dissipation of tidal energy. Their effect on mean water movement is probably negligible.

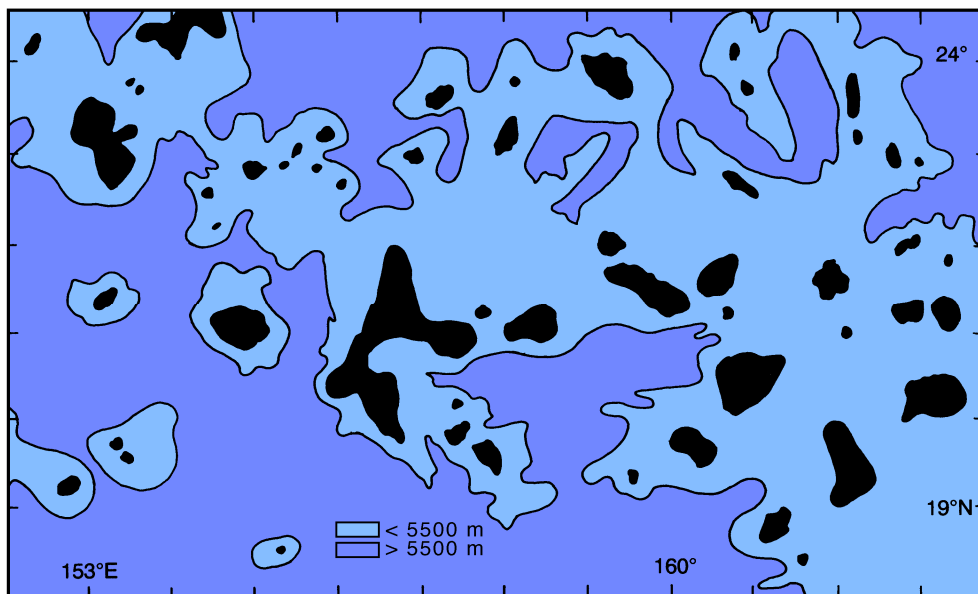


Fig. 8.4. Seamounts in the Northwest Pacific Basin. The 5500 m contour is shown, depths less than 3500 m are indicated in black. The peaks of most shallow structures are less than 2000 m below the sea surface; some of the larger structures may carry more than one peak. Simplified from a GEBCO chart and on the same scale.



China Seas and the region east of the Philippines; these regions thus experience monsoonal climate, with Northeast Monsoon during winter (December - March) and Southwest Monsoon during summer (June - September). The monsoon seasons and winds are the same as in the Indian Ocean, both monsoon systems being in fact elements of the same large seasonal wind system produced by the seasonal heating and cooling of the Asian land mass.

The Intertropical Convergence Zone (ITCZ) is located at 5°N, indicated by a minimum in wind speed (the Doldrums). A second atmospheric convergence known as the South Pacific Convergence Zone (SPCZ) extends from east of Papua New Guinea in a southeastward direction towards 120°E, 30°S. In the annual mean it is not so much seen as a wind speed minimum but more as a convergence in wind direction. Both convergences are regions of upward air movement and thus cloud formation. They are prominent features in satellite-derived maps of cloud cover (Figure 8.5) and will be addressed in more detail when their effect on rainfall and surface salinity is discussed in the following chapter. Contrary to widespread opinion, both the ITCZ and the SPCZ are not regions of no wind; though winds are generally weak, completely calm conditions are encountered during not more than 30% of the year.

### **The integrated flow**

We saw in Chapter 4 how the depth-integrated flow can be derived independently either from atmospheric or oceanic data. We now return to the relevant figures for a more detailed look at the situation in the Pacific Ocean.

Generally speaking, the integrated flow field derived from atmospheric data (Figure 4.4) compares well with the fields derived from oceanic data with different assumed depths of no motion (Figures 4.5 and 4.6). The most prominent feature is the strong subtropical gyre in the northern hemisphere, consisting of (Figure 8.6) the North Equatorial Current with strongest flow near 15°N, the Philippines Current, the Kuroshio, the North Pacific Current, and the California Current. The circulation in the subtropics of the southern hemisphere is weaker; but the gyre is again well resolved from both data sets. The high degree of agreement in the region of weak flow east of 160°W is particularly remarkable: flow away from the Circumpolar Current is northeastward south of 30°S, where it turns northwestward for a while before joining the general westward flow of the South Equatorial Current. This is one of the remotest regions of the world ocean - no shipping lanes pass through it, the distances to ports are too long for most research vessels to reach it, no islands offer refuelling facilities. This makes exploration of this part of the southern subtropical gyre an expensive undertaking. Until more information is obtained from drifting buoys and satellite data, the integrated flow field will remain our best information on currents in the region. Sverdrup dynamics should work particularly well there, and the flow pattern seen in Figures 4.4 - 4.7 should find confirmation from field observations.

More details are revealed in the stream function map (Figure 4.7). It shows the South Equatorial Current, centred around 15°S, and the Peru/Chile Current as major components of the southern subtropical gyre and indicates the existence of western boundary currents along the coasts of Australia and New Zealand. The split near 18°S into the southward flowing East Australian Current and northward flow in the Coral Sea and northward transport across the equator east of Papua New Guinea have been confirmed by recent field observations. The stream function map also reveals the existence of an Equatorial Counter-



current near 5°N, fed from both subtropical gyres. The current's position coincides with that of the Doldrums, where it flows against the direction of the prevailing weak winds.

An indication of a subpolar gyre in the northern hemisphere is seen north of 50°N. Eastward transport in this gyre is again achieved by the North Pacific Current; the circulation is completed by the poleward and westward flowing Alaska Current, the Alaskan Stream, the southern part of the East Kamchatka Current, and the Oyashio.

In summary, the integrated flow indicates the presence of six western boundary currents: the southward flowing Oyashio between 60°N and about 45°N; the northward flowing Kuroshio between about 12°N and 45°N; the inshore edge of the Mindanao Eddy which flows southward from about 12°N to 5°N; a northward flowing unnamed current between 18°S and 5°N; the southward flowing East Australian Current between 18°S and Tasmania; and another southward current along the east coast of New Zealand. Compared to observations, the start and end latitudes for all boundary currents are quite accurate. An exception occurs in the case of New Zealand; observations show that the Tasman Current only travels to the south end of North Island, while a cold current flows northward along South Island. This may be the result of inadequacies in the wind data for the seldom-travelled region east of South Island.

A marked difference between the integrated flow fields derived from atmospheric and oceanic data is seen in the meridional gradients of integrated steric height just to the east of Japan (a similar phenomenon occurs in the north Atlantic Ocean). This difference does not reflect any inadequacy of the wind field; rather, it is a failure of Sverdrup dynamics which assumes broad, slow flow. The Oyashio and Kuroshio are neither broad nor slow, and they meet head-on off Japan. The Kuroshio advects warm water northward, causing steric height to be larger than it otherwise might be within the Kuroshio. Similarly, the Oyashio's advection of cold water reduces steric height below what we would expect from extending the Sverdrup relationship close to the western shore. Thus the gradient between the two is intensified, and the outflow from both boundary currents is narrower and stronger than we would expect from the Sverdrup model. Narrow and strong flow (though still much broader than in reality) is indicated in Figures 4.5 and 4.6 which are based on oceanic observations averaged over many years. In contrast, the wind-based flow fields (Figures 4.4 and 4.7) spread the outflow unrealistically over more than 10 degrees of latitude.

### **The equatorial current system**

When the structure of the circulation is investigated in detail it is found that significant elements of the current field do not show up clearly in the vertically integrated flow. Details of the three-dimensional structure are revealed in field observations, which we shall now review. We divide the discussion into the three major components of the circulation, the equatorial, western boundary, and eastern boundary currents, and begin with the equatorial current system.

Figure 8.7 is a schematic summary of the various elements of the equatorial current system in the Pacific Ocean. It is seen that the system has a banded structure and contains more elements of eastward flow than could be anticipated from the integrated flow field, which indicated only the presence of the North Equatorial Countercurrent. The most prominent of all eastward flows is the *Equatorial Undercurrent* (EUC). It is a swift flowing ribbon of water extending over a distance of more than 14,000 km along the equator with a thickness of only 200 m and a width of at most 400 km. The current core is found at



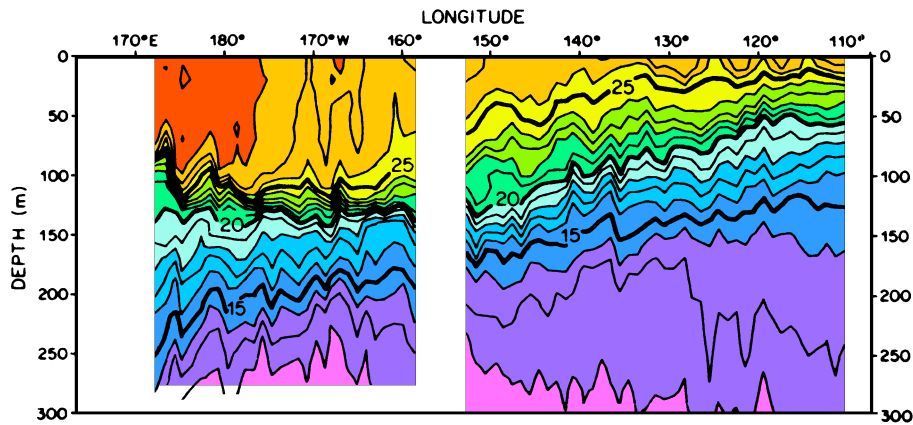


Fig. 8.9. A hydrographic section along the equator. Note the variation in the thickness of the nearly isothermal layer (temperatures above 26°C) from 100 m in the west to less than 20 m in the east, and the upward slope of the thermocline (temperatures between 15°C and 20°C) from west to east from 200 m to 70 m. From Halpern (1980).

In hydrographic sections the EUC is seen as a spreading of the isotherms in the thermocline (Figure 8.8). This weakening of the vertical temperature gradient occurs for two reasons. Firstly, it shows the "thermal wind" character of the Undercurrent (rule 2a in Chapter 3): above about 150 m, eastward current *increases* with depth, and isotherms slope downward on either side of the current; between 150 m and 250 m, eastward current *decreases* with depth, and isotherms slope upward. A second reason becomes apparent when we look at the processes that drive the Undercurrent. We noted in Chapter 3 that at the equator geostrophy works only for zonal flow. This is indeed shown by the fact that the thermal wind equation holds for the Undercurrent, i.e. the *meridional* component of the pressure gradient (indicated by the north-south slope of the isotherms) is in geostrophic balance. But the pressure gradient at the equator also has a *zonal* component, a result of the Trades which dominate the tropics and subtropics from 30°S to 30°N and produce an accumulation of warm water in the western Pacific Ocean. The accumulation of water is evident in any hydrographic section along the equator as a downward slope of the thermocline towards the west (Figure 8.9); according to our rule 1a this indicates a westward rise of the sea surface. The sea level difference between the Philippines and Central America amounts to about 0.5 m and produces a zonal pressure gradient which is unopposed by a Coriolis force. As a result, the current below the wind-driven surface layer accelerates down the pressure gradient (i.e. from west to east) until friction between the current and its surroundings prevents further acceleration of the flow and establishes a steady state. Friction is associated with mixing, and the Equatorial Undercurrent is therefore a region of unusually strong mixing. This leads to a weakening of the gradients normally found in the thermocline and contributes to the observed spreading of isotherms.

Recent observations indicate that in the depth range of the western Pacific thermocline, exchange between the northern and southern subtropical circulation systems is very limited, the separation between the two being located at the southern flank of the North Equatorial



Equatorial Current (Figure 8.11). The transport of the EUC increases downstream, reaching 35 - 40 Sv in the east. Based on the tritium distribution it must be assumed that the water drawn into the EUC along its way also stems mainly from the south. The southern origin of its waters allows the EUC to be identified as a subsurface salinity maximum. Figure 8.12 shows seasonal mean T-S diagrams from the termination region of the Undercurrent. The seasonal variation of salinity at temperatures above 13°C indicates that the EUC flows strongest during January - June but is much weaker in July - December.

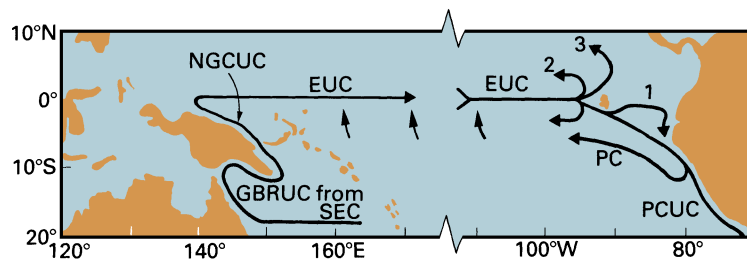


Fig. 8.11. The path of the Equatorial Undercurrent (EUC). SEC: South Equatorial Current. GBRUC: Great Barrier Reef Undercurrent. NGCUC: New Guinea Coastal Undercurrent. PCUC: Peru/Chile Undercurrent. PC: Peru Current (extends to the surface). Flow along path (1) does not occur during July-November. Path (2) is a contribution to the northern flank of the South Equatorial Current, path (3) a smaller contribution to the North Equatorial Current. Based on Tsuchiya *et al.* (1989) and Lukas (1986).

The second most important eastward flow in the equatorial current system is the *North Equatorial Countercurrent* (NECC). It is prominent in the integrated flow which shows it being fed by western boundary currents both from the south and the north (Figure 4.7). Its annual mean transport decreases uniformly with longitude, from 45 Sv west of 135°E to 10 Sv east of the Galapagos Islands. In its formation region the NECC participates in the Mindanao Eddy. At its other end it turns north on approaching the central American shelf, creating cyclonic flow close to the continent. According to rule 2 of Chapter 3 cyclonic motion is associated with a rise of the thermocline in its centre. In the termination region of the NECC this effect is known as the Costa Rica Dome, a minimum in thermocline depth near 9°N, 88°E (Figure 8.13).

The NECC varies seasonally in strength and position. During February - April when the Northwest Monsoon prevents the South Equatorial Current from feeding the NECC (see below) the Countercurrent is fed only from the north. It is then restricted to 4 - 6°N with a volume transport of 15 Sv and maximum speeds below 0.2 m s<sup>-1</sup>; east of 110°W it disappears altogether. During May - January the NECC flows between 5°N and 10°N with surface speeds of 0.4 - 0.6 m s<sup>-1</sup>. It is then fed from both hemispheres, a fact somewhat at odds with the tritium data west of the dateline, which place the separation zone between the circulation of the hemispheres to the south of the NECC and indicate little NECC contact with the southern circulation. The likely answer is that the water that enters the NECC west of 140°E from the south is again lost to the south before reaching the dateline.



decreases to 7 Sv in February. In the eastern Pacific Ocean between 110°W and 140°W horizontal shear between the SEC and the NECC is so large that wave-shaped instabilities develop along the separation zone between the two currents. They are seen as fluctuations of the meridional velocity component and steric height with periods of 20 - 25 days and wavelengths of 1000 km; satellite observations of sea surface temperature show them as cusped waves along the temperature front between the two currents (Figure 8.14). The instability disappears during March - May when the SEC and NECC flow with reduced strength.

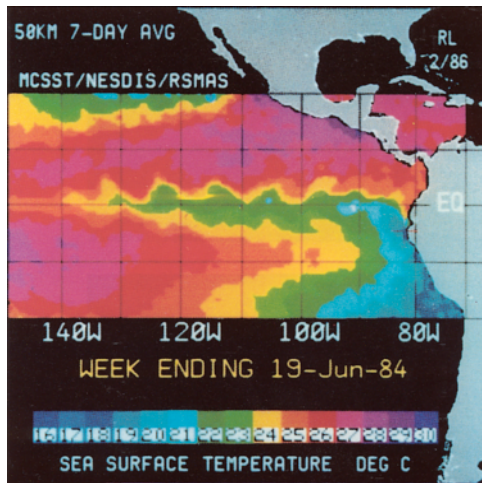
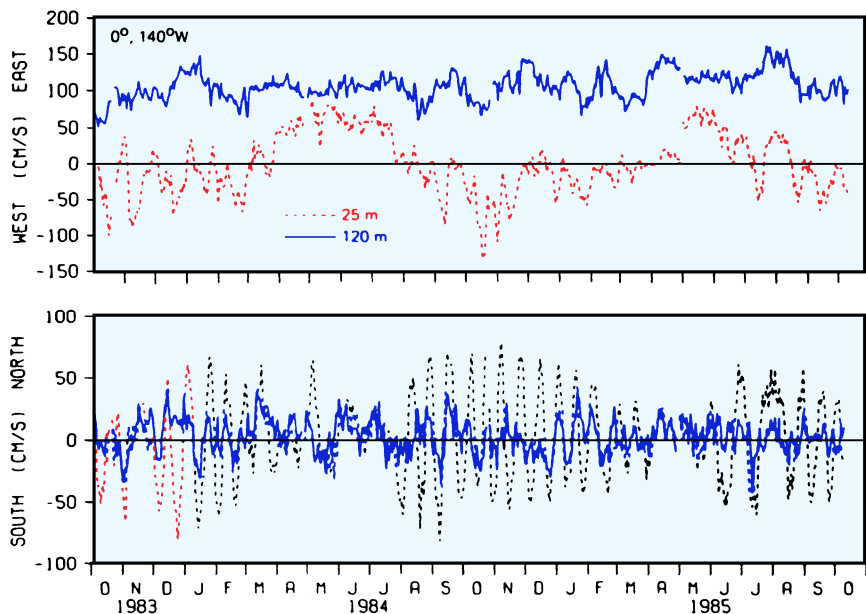


Fig. 8.14. Instabilities at the front between the South Equatorial Current and the North Equatorial Countercurrent in the eastern Pacific Ocean.

(a, left) Satellite image of sea surface temperature in the eastern equatorial Pacific Ocean showing cool water along the equator resulting from upwelling and waves of about 1000 km wavelength in the region of the largest gradient. From Legeckis (1986)

(b, below) Daily means of current components at the equator, 140°W. Note that the 20 - 25 day oscillations do not occur in the Equatorial Undercurrent (120 m level) and are restricted to the meridional component. Note also the absence of oscillations during March - June. From Halpern *et al.* (1988).





The *South Equatorial Countercurrent* is a weak eastward surface current not seen in current maps based on ship drifts but persistently found in results of geostrophic calculations. This may be due to lack of ship traffic, high variability in space and time, or both. Typical surface speeds are below  $0.3 \text{ m s}^{-1}$  at  $170^\circ\text{E}$ , giving a transport of about 10 Sv. Like its northern counterpart the stronger NECC, it is located at a minimum of annual mean wind stress and is therefore strongly seasonal. It is strongest during the Northwest Monsoon (the cause of the wind stress minimum, February - April) and barely seen during winter. In both seasons its strength decreases rapidly east of the dateline (see Figure 8.6), and it may be absent from the eastern Pacific Ocean during most months.

Superimposed on the zonal circulation of Figure 8.6 is weak but important meridional movement. The most important element is at the equator where the Ekman transport in the South Equatorial Current is to the right in the northern hemisphere and to the left in the southern hemisphere. This produces a surface divergence and *equatorial upwelling* in the upper 200 m of the water column. The resulting vertical movement can be determined only by indirect means. Using an array of current meter moorings and applying the principle of continuity of mass between diverging flows it has been estimated as of the order of 0.02 m per day. This is about one order of magnitude smaller than vertical movement in coastal upwelling regions, but the effect is clearly seen in the sea surface temperature (Figures 2.5a and 8.14a). Observations of tritium near the equator are consistent with a vertical transport of 47 Sv, indicating that upwelling is an important element of the current system. The meridional motion associated with the upwelling is also essential for the heat balance of the tropical Pacific Ocean. The heat input received at the surface is balanced by advection of cold water, but zonal advection does not achieve much in that respect in the tropics where the east-west temperature gradients are small. It is therefore mainly meridional advection and upwelling of colder subsurface water that balances the heat input.

In concluding the discussion of the equatorial current system it has to be pointed out that all its elements can change dramatically from one year to the next and that speeds and transports given above are therefore not necessarily representative for particular years. The variations are linked with the ENSO phenomenon which is the topic of Chapter 19. To give an idea of the changes that occur we only mention here that the EUC has been observed to disappear entirely for several months during the mature phase of an ENSO year, while the transport of the NECC increased to 70 Sv - twelve months later it was reduced to 2 Sv. Further discussion of these changes is postponed to Chapter 19.

The *Subtropical Countercurrents* in the region  $20 - 26^\circ\text{N}$  are also permanent features of geostrophic current calculations. They extend to the bottom of the thermocline and often to the 1500 m level. At the surface they can be found in ship drift data with speeds reaching  $0.15 \text{ m s}^{-1}$ . These eastward flows are located in the centre of the subtropical gyre and therefore not strictly part of the equatorial current system; but they are mentioned here for completeness. They do not exist east of the Hawaiian Islands and seem to be a modification of the Sverdrup circulation caused by the presence of that major barrier in the middle of the subtropical gyre - model calculations by White and Walker (1985) indicate that they would not exist if the Hawaiian archipelago were removed. However, banded current structure with alternating eastward and westward flow exceeding  $0.5 \text{ m s}^{-1}$  has also been reported from the region north of the Hawaiian Ridge (Talley and deSzoeke, 1986); so a final explanation remains to be developed. Similar subtropical countercurrents in the southern hemisphere can be expected from the Society Islands and the south Pacific islands further west.



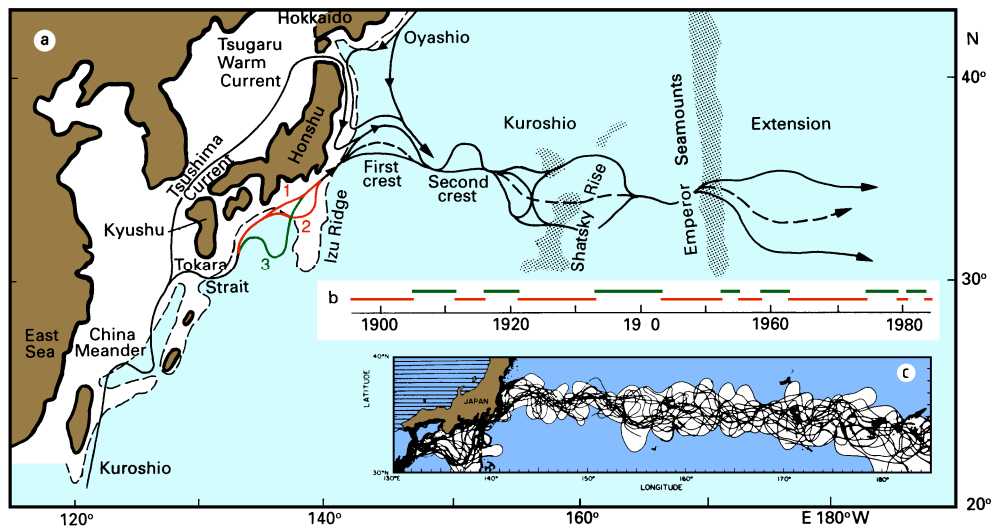


Fig. 8.16. Paths of the Kuroshio and Oyashio. (a) Mean positions of current axis, (b) time history of occurrence of the large meander path south of Japan (the current follows path 3 during the raised portions of the line), (c) individual Kuroshio paths observed during summer 1976 to spring 1980. The broken line is the 1000 m contour and indicates the shelf break. Adapted from Kawai (1972) and Mizuno and White (1983).

In the discussion of geostrophy in Chapter 3 we noted that rule 2 is valid in western boundary currents as long as the hydrographic section is taken across the current axis. The Kuroshio is thus linked with a dramatic rise of the thermocline towards the coast, and a horizontal temperature map at (for example) 300 m depth cuts through the oceanic thermocline near the Kuroshio axis (Figure 8.17). The position of the 15°C isotherm on the 300 m or 200 m level is commonly used as an indicator of the Kuroshio's position. When the temperature map is compared with maps of  $\text{curl}(\tau/f)$  (Figure 4.3) it is seen that the region enclosed by the 15°C isotherm is a region of Ekman transport convergence (downwelling). Sinking motion in the surface layer removes nutrients and keeps biological productivity low despite high levels of sunlight. Ecologically, the central and western regions of the subtropical gyres are the oceanic equivalent of deserts. Devoid of detritus and other organic material, they display the deepest blue of all ocean waters and gave the Kuroshio (which carries their waters north) its name.

The separation point for the Kuroshio is reached near 35°N. It defines the transition from the Kuroshio proper to the Kuroshio Extension. Flow in the Extension is basically eastward, but the injection of a strong jet into the relatively quiescent open Pacific environment causes strong instability. Two regions of north-southward shift, the "First Crest" and the "Second Crest", are found between 140°E and 152°E with a node near 147°E. Both features, as well as the large meander path, are seen in the 300 m mean temperature (Figure 8.17) as features of the long-term mean circulation. East of the Second Crest the Shatsky Rise produces another region of alternative paths. On approaching the Emperor Seamounts the current breaks up into filaments which eventually form elements of the North Pacific Current.



idea that the Kuroshio is the continuation of the North Equatorial Current, which reaches maximum flow in winter. However, the seasonal variation of the wind field and the associated Ekman pumping is not uniform across the tropical Pacific Ocean; and while the variation of NEC transport is in phase with the variation of the wind in the central region, the seasonal wind variation in the western region is in phase with the Kuroshio transport variation. This suggests that a significant part of the Kuroshio transport is wind-generated in the western Pacific Ocean.

North of its separation point the Kuroshio is opposed by the *Oyashio*, the western boundary current of the subpolar gyre. Ekman flow diverges in the centre of this gyre, so the *Oyashio* carries cold water rich in upwelled nutrients and full of marine life - hence its name the "parent current". The two mighty streams meet south of Hokkaido, where the *Tsugaru Warm Current* also brings water from the Japan Sea into the Pacific Ocean (as described in detail in Chapter 10). This water proceeds partly southward along Honshu, while another part moves eastward against the advance of the *Oyashio*. As a result the *Oyashio* generally splits into two paths, called the First and Second *Oyashio* Intrusion (Figure 8.16), and the region to the east of Tsugaru Strait displays extremely complicated hydrography (Figure 8.18). Between one and two anticyclonic (warm-core) eddies are formed each year in the region. Every six years or so one of them grows into a "giant eddy" which then dominates the area for nearly a year.

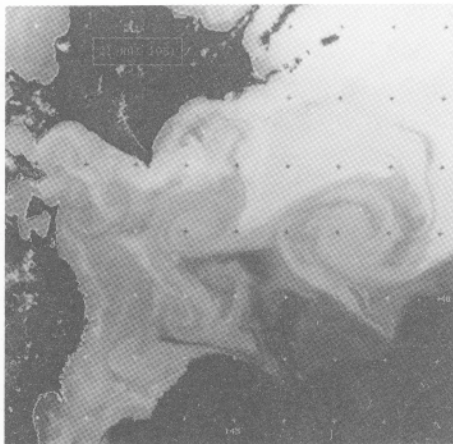


Fig. 8.18. Satellite image of sea surface temperature of the Kuroshio/*Oyashio* frontal region taken on 21 May 1981. The dark area in the southeast indicates very warm water in the Kuroshio. Warm water from the Tsugaru Warm Current enters from the west, through the channel between Honshu in the south and Hokkaido in the north; as indicated by the gray tones it proceeds southward along the Honshu coast. Light tones represent cold water of the *Oyashio*; the First Intrusion is indicated by the coldest water. A large anticyclonic (warm) eddy is centred at 41°N, 147°E. The Second *Oyashio* Intrusion is seen east of the eddy.

The complexity of the region is evident from the figure: Eddies, filaments, and meanders are seen in various stages of formation. In the centre of the observation area a jet-like intrusion from the Tsugaru Warm Current into Kuroshio water produces a "bipole", two small eddies of opposite rotation. (Bipoles are often found at straits or at outlets of strong-flowing rivers. Their eddies are smaller than eddies produced by western boundary currents and differ from them in that they contain the same water mass regardless of their sense of rotation - Kuroshio eddies contain warm water if they rotate anticyclonically but cold water if they have cyclonic rotation.) From Vastano and Bernstein (1984).



months when the region of the Philippines, New Guinea, and northern Australia experiences the monsoon of the southern summer season: during December to March winds over the Philippines blow from the northeast, and from northwest south of the equator (Figures 1.2b and c).

The *East Australian Current* is the western boundary current of the southern hemisphere. Although it is the weakest of all western boundary currents, carrying only about 15 Sv in the annual mean near 30°S, it is associated with strong instabilities. Its low transport volume is partly a consequence of flow through the Australasian Mediterranean Sea; models show that if the Indonesian passage were closed, flow from the Pacific into the Indian

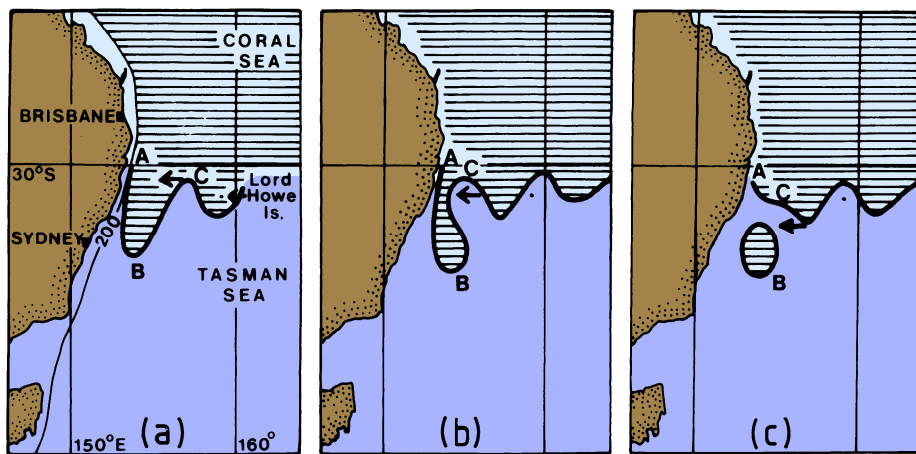


Fig. 8.19 (above). A sketch of eddy formation in the East Australian Current through Rossby wave propagation along the Tasman Front. Point C moves westward towards A. In the process it pinches off the meander and releases current ring B which moves southward. Shading indicates warm Coral Sea water. From Nilsson and Cresswell (1981).

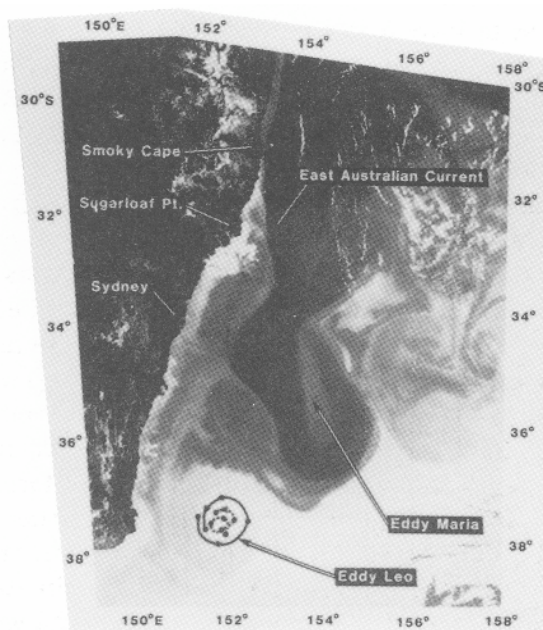


Fig. 8.20 (left). The East Australian Current seen in the sea surface temperature distribution as observed by satellite on 20 December 1980. Dark is warm, light is cold. (Some small scale very light features are clouds.) The tracks in eddy "Leo" are the paths of two drifting buoys. Dots indicate noon positions for each day. From Cresswell and Legeckis (1986).



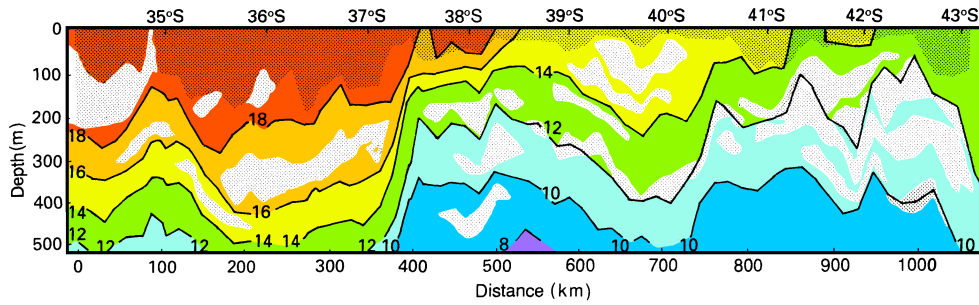
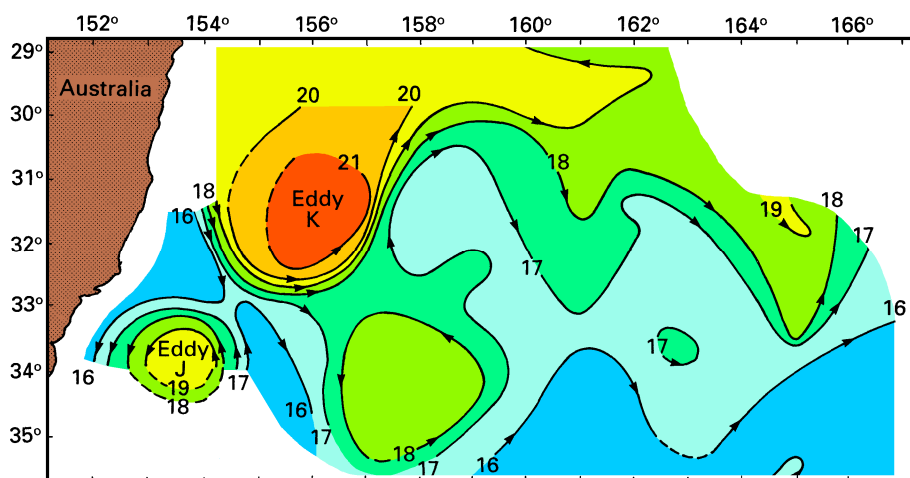
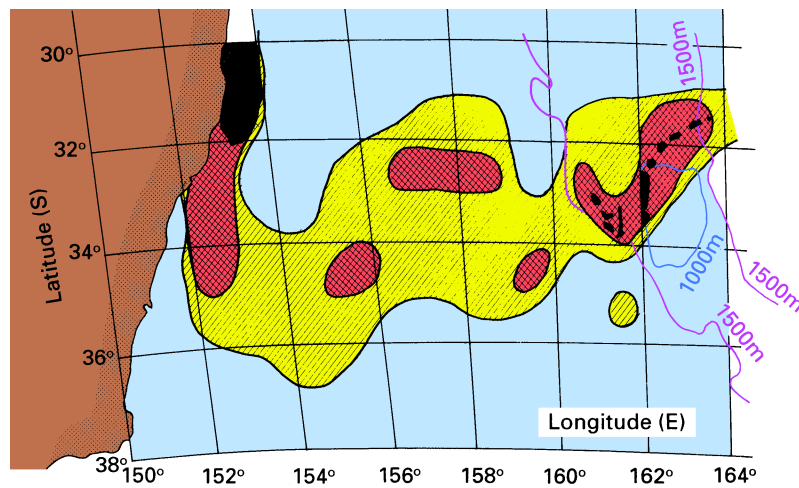


Fig. 8.22. A section of temperature ( $^{\circ}\text{C}$ ) through the Tasman Sea along a track about 150 km seaward of the continental shelf. The shaded regions indicate layers where the temperature changes by less than  $0.1^{\circ}\text{C}$ . In the permanent thermocline where the temperature usually changes by  $0.1^{\circ}\text{C}$  every 5 m, such layers indicate remnants of cores from East Australian Current eddies. From Nilsson and Cresswell (1981).





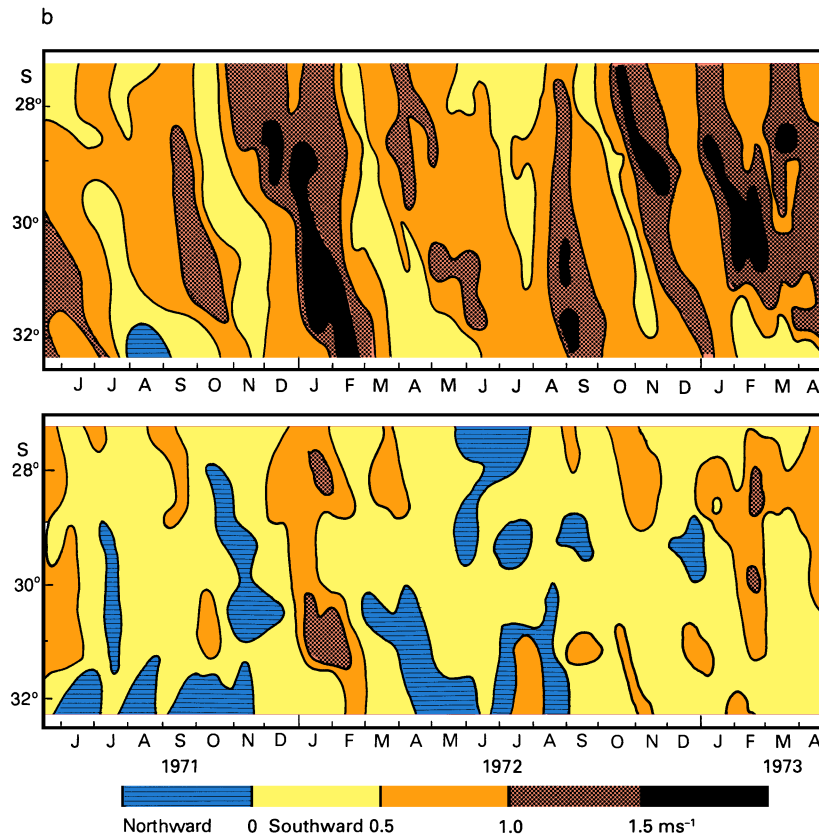


Figure 8.24 (continued). b) current velocity deduced from the drift of southbound vessels (top; mean offshore distance 19 km) and from the drift of northbound vessels (bottom; mean offshore distance 6.5 km) as a function of time. From Godfrey (1973) and Hamon *et al.* (1975). See page 129 for part a of the figure.

The continuation of the East Australian Current east of New Zealand is the *East Auckland Current*. It forms an anti-cyclonic eddy north of East Cape (near 37°S) similar in size and with the same homogeneous deep core as the eddies in the Tasman Sea; the eddy is, however, apparently topographically controlled, being found at the same location throughout the year. There is evidence that the East Auckland Current undergoes seasonal change; during summer most of its transport continues as the *East Cape Current* and follows the New Zealand shelf southward until it reaches the Chatham Rise, while during winter some of it separates from the shelf and continues zonally into the open ocean, forming a temperature front near 29°S. Another shallow front near 25°S, sometimes referred to as the Tropical Front, marks the northern limit of eastward flow in the subtropical gyre. At the surface, the westward flow of the South Equatorial Current rarely extends more than 300 km to the south of Fiji (i.e. 20°S); but the boundary between eastward and westward flow slopes down to the south, and at 800 m depth it is found more at 30°S (Roemmich and Cornuelle, 1990).



balance. The cross-stream pressure gradient adjusts itself to geostrophic balance with the undercurrent, which can therefore be seen in a downward tilt of the isotherms and isohalines toward the shelf below the surface layer. At the surface, the upward tilt of the isotherms and eventual surfacing of the thermocline gives rise to a front which, through geostrophic adjustment, produces an intensification of the flow known as the coastal jet *CJ*.

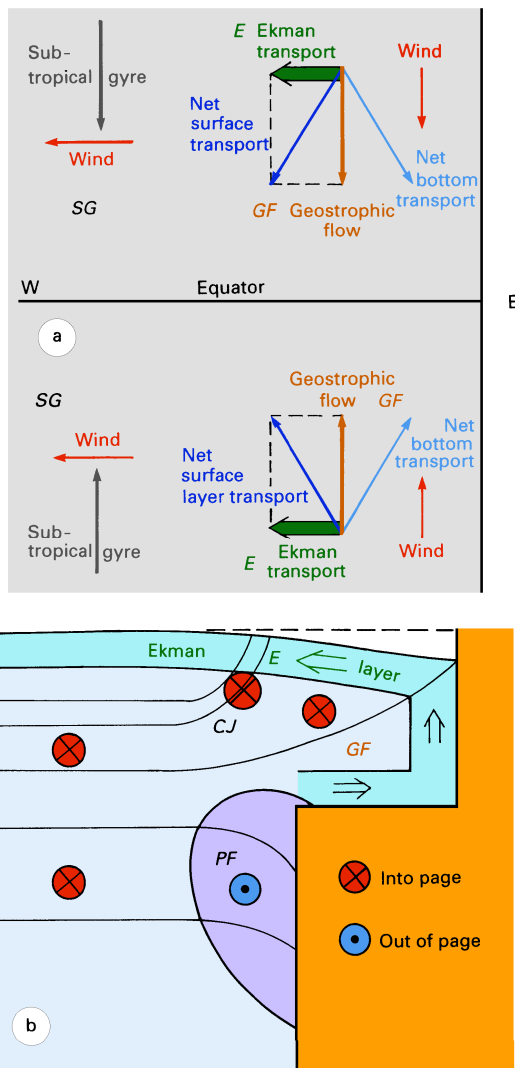


Fig. 8.25. Dynamics of coastal upwelling regions.

(a) plan view,

(b) vertical section (southern hemisphere).

The thin lines in (b) represent isotherms or isopycnals. See text for details.

The upwelling circulation just described is embedded in the much broader equatorward flow of the subtropical gyre circulation *SG*. At the surface the two circulation systems combine to advect cold water towards the tropics, lowering the sea surface temperature along the eastern boundary. The result is a deflection of isotherms from zonal to meridional



toward the coast of the isotherms below 100 m indicates geostrophic adjustment of the density field to the undercurrent along the slope.

Coastal upwelling systems are among the most important fishing regions of the world ocean because they offer optimum conditions for primary production. The basis for all marine life is photosynthesis in phytoplankton, which can only occur in a layer as deep as sunlight can reach (the so-called euphotic zone, which is less than 200 m deep even in very clear water and usually much shallower). The other requirement are nutrients to support phytoplankton growth. They are supplied by remineralization of dead organisms. In contrast to the nutrient cycle on land, where dead organisms are composted and the nutrients returned to the soil, the nutrient cycle in the open ocean is not very efficient: Much of the nutrient reservoir is locked below the euphotic zone because dead organisms sink and escape from the euphotic zone before they can be remineralized. Coastal upwelling regions are among the few regions of the world ocean where nutrients are returned to the surface layer and made available for phytoplankton growth. This forms the basis for a marine food chain with high productivity. All coastal upwelling regions therefore support important fisheries.

The Peru/Chile upwelling system is the most productive coastal upwelling region of the world ocean. It extends from south of 40°S into the equatorial region where it blends into the equatorial upwelling belt. Despite its vast resources, human greed managed to destroy the basis of what before 1973 was the largest fishery in the world. Overfishing and natural variability of the upwelling environment brought about the end of an industry. This aspect of the Peru/Chile Current System will be taken up again in Chapter 19.

Considerable uncertainty exists about the details of the flow field in the southern part of the Peru/Chile Current. The upwelling undercurrent is known to extend from at least north of 10°S to 43°S and possibly beyond, decreasing in strength from some  $0.1 \text{ m s}^{-1}$  in the north to barely more than  $0.02 \text{ m s}^{-1}$  in the south. Further offshore a conspicuous feature is a surface salinity minimum along 40°S (Figure 2.5b). It is known that rainfall along the coast is large in the region; but it can easily be shown that rainfall alone cannot explain the observed salinity minimum. Some researchers conclude that westward flow against the prevailing direction of the subtropical gyre circulation must occur in the region. This may explain why the Subtropical Front is displaced so far northward in the Pacific Ocean off South America and ill defined.

The corresponding coastal upwelling region in the northern hemisphere is found in the *California Current*. Its vast living resources are known from John Steinbeck's novel "Cannery Row" set in Monterey, the centre of the sardine fishery before it collapsed from overfishing in the 1930s. Winds along the coast are much more seasonal here than along the coasts of Peru and Chile (Figure 1.2). Equatorward winds prevail along the coast of Washington, Oregon, and California from April into September, while during the remainder of the year winds are variable and often southeasterly. As a result, poleward flow at the surface is observed during October - March over the shelf and even further offshore. This seasonal flow, which reaches its peak with  $0.2 - 0.3 \text{ m s}^{-1}$  in January - February, is often called the *Davidson Current*. Coastal upwelling with equatorward surface flow prevails during spring and summer, lowering the sea surface temperatures along the coast to 15°C and less at a time when only kilometres away the heat on land is hardly bearable. The associated cooling of the air leads to condensation, and a coastal strip usually less than a kilometre wide is nearly permanently shrouded in sea fog - the postcard photographs of the famous Golden Gate bridge spanning a blue San Francisco Bay in bright sunshine cannot



be taken until October when the upwelling ends and sea surface temperatures reach their annual maximum. Even during the upwelling season poleward flow prevails along the coast of southern and central California in an inshore strip of up to 100 km width, apparently as part of a large cyclonic eddy between the California Current and the coast which has been observed to exist throughout the year except during March and April. Further north, inshore poleward flow with velocities in excess of  $0.3 \text{ m s}^{-1}$  can exist during periods of weak winds but is suppressed if the upwelling is strong.

High variability of winds and upwelling intensity are a characteristic feature of the Californian upwelling system. Figure 8.27 shows the circulation during a period of weak wind and a period where winds were particularly strong. The competing influences of wind-driven equatorward flow and poleward flow driven by the alongshore pressure gradient are seen in the weakening of the undercurrent as the wind increases.

North of the Californian upwelling region is the *Alaska Current*, also called the Alaska Coastal Current, the eastern component of the subpolar gyre. Freshwater input from Alaska's rivers reduces the density in the upper layers near the coast, enhancing the pressure gradient across the current and constraining the current path to the coastal region. As a consequence, the current is concentrated on the shelf. It is strongest in winter when it shows speeds of up to  $0.3 \text{ m s}^{-1}$  and weakest in July - August when the wind tends to oppose its flow (Figure 1.2). During some years flow east of  $145^\circ\text{W}$  ceases altogether during these months and the subtropical gyre is displaced some 700 km westward (Royer and Emery, 1987). Eddies may then dominate the region along the Canadian/Alaskan coast. A well defined anticyclonic eddy has been reported from buoy tracks and cruise data off Sitka (Figure 8.28) with average surface speeds exceeding  $0.7 \text{ m s}^{-1}$ . The eddy exists during spring and summer and possibly throughout the year. It reaches to at least 1000 m depth, although its speed is reduced by half at 200 m.

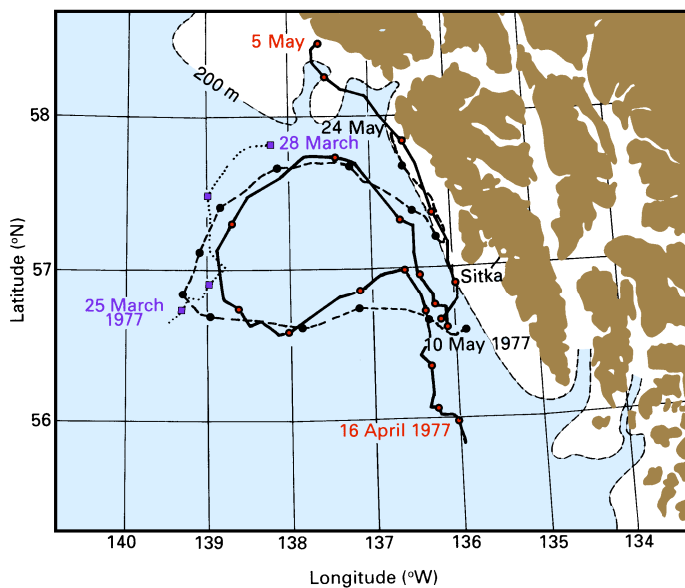


Fig. 8.28. The anticyclonic eddy off Sitka as seen in the trajectories of three satellite-tracked buoys during March - May 1977. From Tabata (1982).